Simulation of the energy-band structure of superlattice of quaternary alloys of diluted nitrides

© A.S. Dashkov[1], N.A. Kostromin[2], A.V. Babichev[3], L.I. Goray[1], A.Yu. Egorov[1]

[1] Alferov Federal State Budgetary Institution of Higher Education and Science
Saint Petersburg National Research Academic University of the Russian Academy of Sciences,
194021 St. Petersburg, Russia
[2] Peter the Great Saint-Petersburg Polytechnic University,
195251 St. Petersburg, Russia
[3] ITMO University,
197101 St. Petersburg, Russia

E-mail: dashkov.alexander.om@gmail.com

Received September 30, 2022
Revised March 10, 2023
Accepted May 2, 2023

The paper describes an algorithm for computing the interband transition energy for superlattices of quaternary solid solutions of diluted nitrides. Using the described method, the authors have conducted several numerical simulations of test structures with InGaAsN quantum wells for the method verification using experimental data and comparison with other approaches. Simulation results showed the validity of the used approach. The hybridization parameter estimation method for Indium mole-fraction below 30% is presented. Based on simulation results, the authors propose InGaAs/GaAsN superlattices' parameters for the implementation of the source emitting in the 1.3 μm spectral range

Keywords: superlattices, diluted nitrides, interband transitions, numerical simulations, hybridization parameter.

DOI: 10.21883/SC.2023.03.56237.4163

1. Introduction

Quaternary solid solutions $A^{III}B^{V}$ based on „dilute" nitrides ($In_yGa_{1-y}N_xAs_{1-x}$ with a nitrogen content of diluted x up to 5%) allow to reduce the band gap by changing the nitrogen content at a constant indium content [1]. This effect opens up prospects for the use of InGaAsN layers grown on GaAs substrates in the creation of long-wavelength (in the 1.3 μm spectral range) devices of optoelectronics and photonics [1–3] (solar cells [4], bipolar transistors [2], lasers [5]). In particular, structures based on InGaAsN are promising from the point of view of the implementation of monolithic vertically emitting lasers (VCSEL) with a spectral range of 1.3 μm on GaAs [6–9] substrates. The latest results of research in this direction are reflected in the paper [10]. Moreover, the additional introduction of Sb into the layers of nitrogen-containing active regions (the use of GaInNAsSb quantum wells, QWs) allows to implement VCSEL in the spectral range 1.55 μm on GaAs [3] substrates. Meanwhile, due to the relatively low optical gain of nitrogen-containing QWs, VCSELs based on them demonstrate a low output optical power, which ultimately limits their modulation characteristics.

One of the approaches to increase the modal gain of monolithic long-wavelength VCSEL, along with the use of highly mechanically stressed QW [11,12], is the use of short-period superlattices (SL). Previously, the results on the creation of long-wavelength VCSEL obtained by the technology of wafer sintering [13–15] with an active area based on $In_{0.57}Ga_{0.43}As/In_{0.53}Ga_{0.20}Al_{0.27}As$ SL, as well as metamorphic VCSEL with active area based on $In_{0.41}Ga_{0.59}As/In_{0.25}Ga_{0.75}As$ SL [16].

This paper presents the results of a numerical calculation of the transition energy in active regions based on nitrogen-containing SL to create monolithic VCSEL in the spectral range 1.3 μm on GaAs substrates. Application of SL instead of InGaAsN QWs allows not only to increase the modal enhancement of VCSEL active regions, but also prevents the layer interdiffusion effect, which is typical for active regions based on InGaAsN QWs after high-temperature annealing [17].

2. Technique of the numerical experiment

Calculation of the energy of interband transitions in the SL was determined in several steps. The first step was to construct the profile potentials of the top of the valence band and the bottom of the conduction band, and numerically solve the Schrödinger equation (SE) for both potentials. The result of the numerical calculation — the position of the energy levels and the form of the wave functions corresponding to them (near the Γ-point in the k-space) [18–20]. The resulting wave functions were used to calculate the magnitude of the dipole interaction matrix elements. The data presented in the paper [21] were used as input data (main energy and mechanical parameters) for the presented calculations.

2.1. The electron potential profile

The calculation of the SL electron potential profile (the top of the valence band, the bottom of the conduction band), omitting the corrections related to the strain of the structure, was reduced to one of two types of calculation:
— calculation of potentials for ternary, quaternary solid solutions of compounds $A^{III}B^{V}$containing no nitrogen ($In_yGa_{1-y}As$, $Al_xIn_yGa_{1-x-y}As$);
— calculation for quaternary solid solutions with a small fraction of nitrogen ($In_yGa_{1-y}N_xAs_{1-x}$).

The first type of calculations was implemented as a simple model. Based on the value of the desired energy parameter (P) for materials $A^{III}B^{V}$, using Vegard's law [22], the values of the required parameter for quaternary solid solutions were obtained in the general case. The accuracy of the obtained energy parameter, the potential, in this case directly depends on the accuracy of the used energy parameters of binary materials, determined with high accuracy for a number of materials [21].

For the case of quaternary solid solutions of the form $In_yGa_{1-y}N_xAs_{1-x}$, the linear approximation used in Vegard's law is not applicable to the potential of the bottom of the conduction band. As shown earlier [1], at low nitrogen fractions, the initial conduction band splits into two branches with energies E^+ and E^-. Meanwhile, the nitrogen impurity has practically no effect on the position of the top of the valence band [23]. As a result, to calculate the energy parameters (the energy position of the branches of the conduction band), the model of interaction between two energy bands (Band AntiCrossing, BAC model) [1,24] is used. And to calculate GaNAsSb solid solutions, a similar extended approach (double BAC model) [25–27] is used. The advantage of the BAC model is that it allows using simple analytical expressions to determine the position of the branches of the conduction band under the assumption that the residual mechanical stresses are small:

$$E_{\pm} = \frac{1}{2}\left(\left[E^C(k) + E^L\right] \pm \sqrt{\left(E^C(k) - E^L\right)^2 + 4V^2x}\right), \quad (1)$$

where E^C — dispersion of the conduction band of the compound the atoms of which are being replaced, E^L — energy of localized states of substituting atoms (nitrogen), V — hybridization parameter.

2.1.1. The parameters of the BAC model

The accuracy of the calculated energy position of the bottom of the conduction band for „diluted" nitrides directly depends on the accuracy of determining the parameters E^L and V. The values of these parameters are recovered from the experimental data for each given diluted quaternary solid solution [1]. Meanwhile in different literary sources of the same declared chemical composition, different values E^L and V [28] are often presented. These differences can be due to a number of reasons: small deviations of the true composition from the declared one; the presence of unaccounted mechanical stresses in the layers of the structure; internal difference in the structure of the layers of the solid solution.

As shown previously [28], the last factor is the most significant. The calculations carried out via tight-binding method showed that the nearest environment of nitrogen atoms can be represented as five different configurations, each of which is characterized by different values of E^L and V. As a result, the type of configuration which will be realized in the structure under study depends both on the chemical composition (indium fraction y) and on the conditions under which the epitaxy and post-growth processing of the samples took place. In particular, when using the method of metalorganic vapour phase epitaxy Ga−N bonds are predominantly formed [28]. Nevertheless, the most energetically favorable configuration is one in which all the nearest neighboring nitrogen atoms are indium atoms (4In) [28,29]. In the case of structure annealing, a structural transition to this configuration occurs, which is confirmed by an increase in the band gap after high-temperature annealing of the [28,29] structures. Therefore, the parameters for the 4In configuration were used in the calculations.

Thus, to determine the values of the parameters E^L and V, quadratic interpolation obtained on the basis of selected experimental data was used. For the parameter E^L, the interpolation was [30]:

$$E^L = 1.65(1-y) + 1.44y - 0.38y(1-y). \quad (2)$$

For the parameter V, a quadratic interpolation was constructed with fixed edge values at the points corresponding to GaAsN and InAsN. However, unlike the interpolation suggested in [30]:

$$V = 2.7(1-y) + 2.0y - 3.5y(1-y)$$
$$= 3.5y^2 - 4.2y + 2.7, \quad (3)$$

the experimental values were supplemented with updated data [31–45] and taken into account when constructing the interpolation with weight coefficients. So, if for the same composition in the literature there were several (N) values of the Vparameter, then each of them was taken with the weight $1/N$. The result was the interpolation of the form (see Fig. 1):

$$V = 0.773y^2 - 1.473y + 2.7. \quad (4)$$

The obtained interpolation, as before, still does not give complete agreement with all experimental data (Fig. 1, Table 1) [46–52], however, it allows to reduce discrepancies compared to the results obtained with interpolation by expression (3) (see Table 1).

2.2. Accounting for corrections due to mechanical stress in the layers of the structure

In the above numerical calculation, corrections associated with mechanical stress in the SL structure were taken into

Table 1. Comparison of the experimental (from PL peak position, measured at a temperature of 300 K) and theoretical values of the interband transition energy for test structures based on InGaAsN QWs, calculated on the basis of the proposed interpolation (ΔE_{th1}) and the previous one (ΔE_{th2})

№ structure	structure	$\Delta E_{\exp}$, eV	ΔE_{th1}, eV	ε_{th1}, %	ΔE_{th2}, eV	ε_{th2}, %
1	$In_{0.3}Ga_{0.7}As_{0.992}N_{0.008}$–GaAs QW [46]	0.99	1.14	14.1	1.18	18.1
2	$In_{0.05}Ga_{0.95}As_{0.98}N_{0.02}$–GaAs QW [47]	1.17	1.21	3.4	–	–
3	$In_{0.3}Ga_{0.7}As_{0.996}N_{0.004}$–GaAs QW [48]	1.06	1.19	12.3	1.22	15
4	$In_{0.36}Ga_{0.64}As_{0.983}N_{0.017}$–GaAs [49]	0.985	1.05	6.5	1.12	13.7
5	$In_{0.36}Ga_{0.74}As_{0.981}N_{0.019}$–GaAs [50]	0.972	1.08	11.1	1.13	16.2
6	$In_{0.3}Ga_{0.7}As_{0.972}N_{0.028}$–GaAs [50]	0.972	1.08	11.1	1.15	18.3
7	$In_{0.35}Ga_{0.65}As_{0.92}N_{0.018}$–GaAs [51] 3 QW	0.999	1.05	5.1	1.10	10.1
8	$In_{0.033}Ga_{0.012}As_{0.012}N_{0.012}$–$GaAs_{0.012}N_{0.012}$ QW [52]	0.98	0.96	2	0.96	2

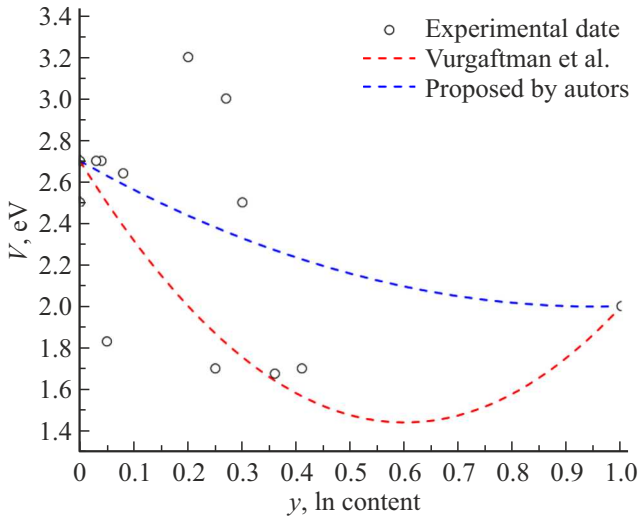

Figure 1. Dependence of the hybridization parameter V on the mole fraction In. Experimental data [31–45] are represented by dots, interpolation curves: red dotted line — proposed earlier in the paper [30], blue dotted line — proposed by the authors of this work.

account. Taking into account the strain tensor $\varepsilon_{i,j}$, the shift corrections to the position of the bottom of the conduction band and the top of the valence band are presented as [53]:

$$\delta E_{E_c} = a_c Sp\hat{\varepsilon}, \tag{5}$$

$$\delta E_{E_v} = a_v Sp\hat{\varepsilon}, \tag{6}$$

where $Sp\hat{\varepsilon} = \varepsilon_{xx} + \varepsilon_{yy} + \varepsilon_{zz}$ — the strain tensor trace.

The components of the strain tensor for a stressed layer can be expressed in terms of the lattice constants of the layer a_l and the substrate a_0, as well as in terms of the elastic constants of the material c_{11}, c_{12}:

$$\varepsilon_{xx} = \varepsilon_{yy} = \frac{a_0 - a_l}{a_l}, \tag{7}$$

$$\varepsilon_{zz} = -\frac{2c_{12}}{c_{11}}\varepsilon_{xx}. \tag{8}$$

Taking into account the differences in the symmetry of the states of the valence band and the conduction band, as well as the spin-orbit interaction, using the Beer–Pikus Hamiltonian, the final corrections to the position of the bottom of the conduction band and the top of the valence band can be expressed as follows [53]:

$$E^{\Gamma}_{C-HH} = E^{\Gamma}_g + \delta E_{E_c} + \delta E_{E_v} - Q_\varepsilon, \tag{9}$$

$$E^{\Gamma}_{C-LH} = E^{\Gamma}_g + \delta E_{E_c} + \delta E_{E_v} + \frac{1}{2}\left(Q_\varepsilon - \Delta_{SO} + \sqrt{\Delta^2_{SO} + 2\Delta_{SO}Q_\varepsilon + 9Q^2_\varepsilon}\right), \tag{10}$$

$$E^{\Gamma}_{C-SO} = E^{\Gamma}_g + \delta E_{E_c} + \delta E_{E_v} + \frac{1}{2}\left(Q_\varepsilon - \Delta_{SO} - \sqrt{\Delta^2_{SO} + 2\Delta_{SO}Q_\varepsilon + 9Q^2_\varepsilon}\right), \tag{11}$$

where Δ_{SO} — spin energy of the orbital splitting without deformation, and the shear deformation potential b is included in Q_ε

$$Q_\varepsilon = \frac{b}{2}\cdot(\varepsilon_{xx} + 2\varepsilon_{yy} - 2\varepsilon_{zz}). \tag{12}$$

2.3. Numerical solution of the Schrödinger equation

To find the energy eigenvalues for a given potential and the effective mass of the electron and hole, „shooting“ method [54,20]) and „finite element“ method (FEM — [20]) were used. In case of using the shooting method, the values of the wave function were determined by the method of transfer matrices, and the energy eigenvalues were determined by the bisection method. It should be mentioned that the final implementation was not the classical transfer matrix method, but its modified version [55], to eliminate the potential numerical instability of the classical method. To solve SE, the value of the effective electron mass was

Table 2. Comparison of the theoretical values of the interband transition energy for test structures based on InGaAsN QWs calculated using the shooting method (ΔE_{sh}) and the finite element method (ΔE_{fem})

№ structure	Structure	ΔE_{exp}, eV	ΔE_{sh}, eV	ΔE_{fem}, eV	ε_{sh}, %	ε_{fem}, %
1	$In_{0.3}Ga_{0.7}As_{0.992}N_{0.008}$ – GaAs QW [44]	0.99	1.14	1.13	14.1	14.1
2	$In_{0.05}Ga_{0.95}As_{0.98}N_{0.02}$ – GaAs QW [45]	1.17	1.21	1.22	3.4	4.2
3	$In_{0.3}Ga_{0.7}As_{0.996}N_{0.004}$ – GaAs QW [46]	1.06	1.19	1.19	12.3	12.3
4	$In_{0.36}Ga_{0.64}As_{0.983}N_{0.017}$ – GaAs [47]	0.985	1.05	1.06	6.5	7.6
5	$In_{0.36}Ga_{0.74}As_{0.981}N_{0.019}$ – GaAs [48]	0.972	1.08	1.07	11.1	10
	Mean deviation				9.5	9.6

determined on the basis of the expression

$$\left(m^*(x, E_q)\right)^{-1} = (m_0)^{-1} \times \left\{1 + 2F + \frac{E_p}{3}\left[\frac{2}{E^{\Gamma}_{C-LH} + E_q} + \frac{2}{E^{\Gamma}_{C-SO} + E_q}\right]\right\}, \quad (13)$$

where F — the Kane parameter representing the 2-nd-order perturbation term of the $\mathbf{k} \cdot \mathbf{p}$ theory, E_p — matrix element of the momentum between s-like conduction bands and p-like valence bands in energy units, E_q — energy quantization of the energy of states above or below the conduction band. The effective mass of holes was determined using the Luttinger parameters under the assumption that small fractions of nitrogen do not affect the parameters of the valence band, in particular, the effective mass of holes [23,30]. The Bastard boundary conditions [20] were used as the boundary conditions at the barrier/well interface. In case of the finite element method, the position of the energy and the wave functions were determined by numerically solving the problem of the eigenvalues of the matrix of the corresponding Hamiltonian without taking into account the degree of nonparabolicity. The modeling procedure in both cases was implemented as a program code in Python3™, parameters were interpolated using the SciPy© library, the problem of finding eigenvalues — was solved using the NumPy© library. To speed up the numerical calculation twice, the program execution process was divided into two sub-processes for finding the energy eigenvalues for each of the potential profiles and into four sub-processes for finding the wave functions corresponding to discrete energy levels.

To demonstrate the applicability of the approach, the results obtained by both methods are presented in Table 2. But the ultimate goal was to use the shooting method, due to its lower asymptotic complexity [20], which is an important factor in modeling, in particular, in optimizing SL and quantum-cascade structures [20].

3. Results and discussion

To test the developed calculation algorithm, simulation of the test structures of InGaAsN quaternary solid solutions was carried out with a known radiation energy (peak position in the experimental photoluminescence spectrum (PL)). The calculation was carried out in several steps:

— the input data of the structure were inputted: chemical composition (mole fractions), period parameters (thicknesses) SL;

— an energy diagram and wave functions were plotted for the obtained energy eigenvalues in SE;

— dipole interaction matrix elements were calculated from the obtained wave functions to determine the most probable transitions.

The simulation of multi-period SL in the implementation within the framework of the shooting method was limited to the simulation of six periods of the corresponding lattice. A further increase in the number of periods did not affect the position of the electronic energy levels and the shape of the wave functions. For a smaller number of periods, the difference in the position of the levels was $\sim 1\%$.

Structures based on $In_yGa_{1-y}N_xAs_{1-x}$ QWs with a fraction of indium $y \leq 0.3$ [46–52] were used as test structures. The results obtained during the simulation are presented in Tables 1 and 2. It is shown that the final error of determination in the calculation method used does not exceed 14%, compared to 18% for the method proposed earlier [30]. In addition, for the structure 2 presented in Table 1, numerical experiments were carried out to determine the nature of the dependence of the transition energy on the QW thickness. It is shown that the largest deviation of the calculation from the experimental value is achieved at a QW thickness of 8 nm and amounts to 5%. The obtained dependence, shown in Fig. 2 together with the experimental data, indicates that the calculated values also fall (with a small total deviation) on the approximation curve, which has an inverse quadratic dependence on the QW thickness. This type of the dependence was proposed for the experimental points in the paper [47].

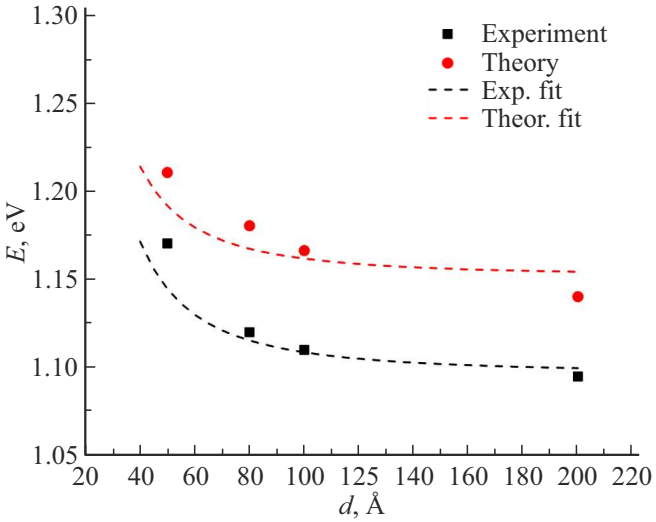

Figure 2. Dependence of the experimental and calculated transition energy for a structure based on $In_{0.05}Ga_{0.95}As_{0.98}N_{0.02}$ QW [47] on the thickness of the quantum well. Dashed lines — result of point approximation of calculated and experimental values [47].

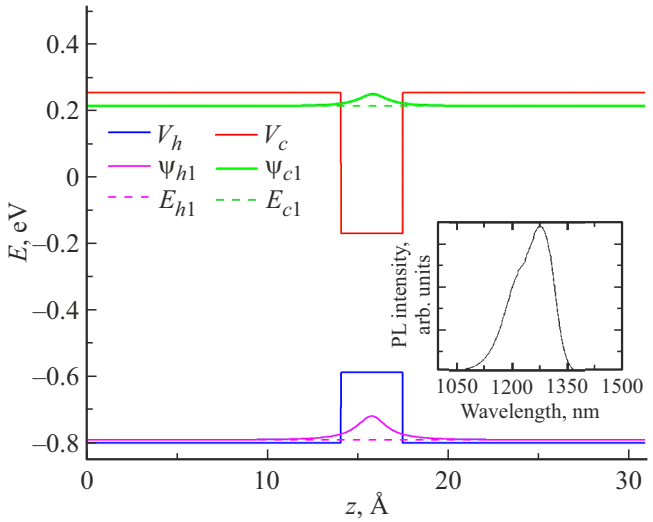

Figure 3. The profile of the bottom of the conduction band and the top of the valence band, as well as the energy eigenvalues E_{ci}, E_{hi} and the corresponding wave functions for one period of the SL2 structure. (A color version of the figure is provided in the online version of the paper).

After testing the approach on test structures based on InGaAsN QWs, a verification calculation of the transition energy of the active region based on a nitrogen-containing SL was carried out. This calculation considered SL1, of composition $InAs/GaAs_{0.966}N_{0.034}$ with layer thicknesses of 0.34/2.82 nm, respectively, studied earlier experimentally in the paper [54]. The photon energy for this SL was 0.96 eV according to the results of measuring the PL spectrum.

The energy diagram, discrete energy levels and wave functions for a given SL are shown in Fig. 3. The transition energy $e_1 - hh_1$ was 1.00 eV, which agrees with the experimentally obtained value of 0.96 eV (corresponding to the radiation wavelength of 1276 nm). The calculation error for SL1 was $\sim 4\%$. A similar calculation was made using the finite element method — the deviation from the values calculated above was ~ 4 meV.

Thus, it was shown that there is sufficient compliance with the energy of the optical transition and the peak position of the PL spectrum. The use of potential barriers with a thickness of ~ 3 nm provides PL in the spectral range $1.25-1.27\,\mu$m, required to create a VCSEL in the spectral range $1.3\,\mu$m.

To determine the parameters of SL emitting in the required spectral range on the basis of alternative compositions and thicknesses, additional numerical experiments were carried out with varying thicknesses and compositions of SL layers. However, the search space for optimal parameters in this case turns out to be too large for research,

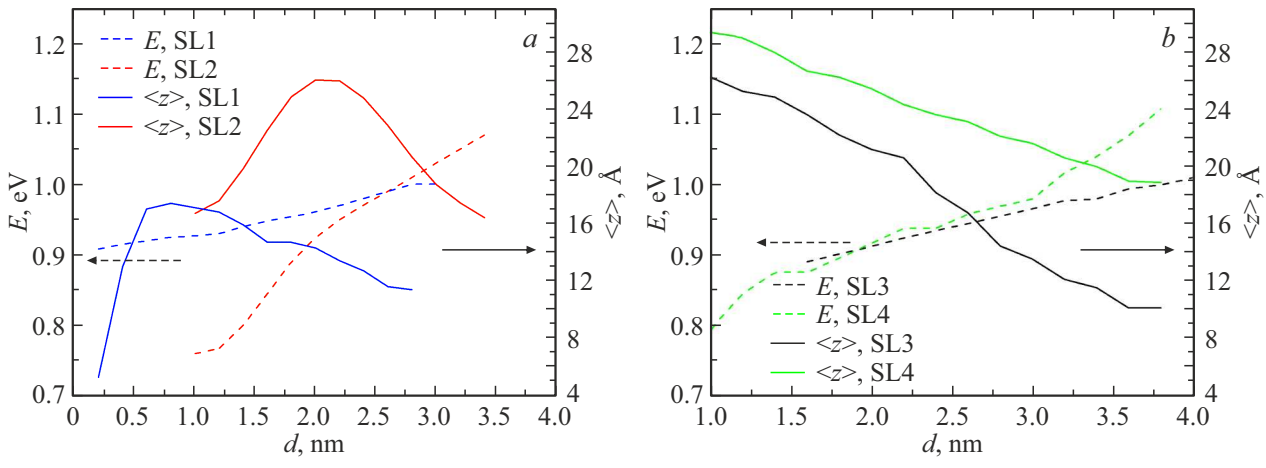

Figure 4. Dependence of the main transition energy and the value of the dipole matrix element for structures SL1 (SL1) and SL2 (SL2) (*a*); SL3 (SL3) and SL4 (SL4) (*b*).

and it was decided to narrow it down: several types of SL were considered, differing in the composition of the layers; for each type of SL, restrictions on the layer thicknesses were additionally introduced.

In all cases SL consisting of GaAsN/In(Ga)As layers were considered. The mole fraction of nitrogen in the GaAsN layers was selected based on the analysis of the peak in the PL spectra [56,57]. For the mole fraction of indium in In(Ga)As, two compositions have been proposed: InAs (SL1, SL3) and $In_{0.8}Ga_{0.2}As$ (SL2, SL4). The first option was considered due to the fact that there were already experimental results indicating the presence of a transition energy in the required range [54]. The second composition was proposed as an alternative with a smaller proportion of indium. The limitation on the thickness of the InGaAs layer was due to the complexity of growing thick planar layers of this composition [58].

For the SL1 structure, the barrier layer thicknesses were varied in the range $d = 0.30-2.82$ nm [59]. Similar calculations were performed for $GaAs_{0.966}N_{0.034}/In_{0.8}Ga_{0.2}As$ (SL2) with a QW layer thickness of 0.30 nm (one monolayer) and barrier layer thicknesses $d = 1.00-4.96$ nm.

The structures of SL3 were additionally considered ($GaAs_{0.966}N_{0.01}$/InAs), SL4 ($GaAs_{0.966}N_{0.01}/In_{0.8}Ga_{0.2}As$) with a similar variation in the barrier layer thickness and a QW layer thickness of 0.30 nm. A smaller mole fraction of nitrogen in the barrier layers of these SL was chosen to reduce the tension and defectiveness of the structures [60,61].

The results of numerical calculations are presented in Fig. 4. It is shown that the required quantum energy (0.97–0.99 eV) can be achieved for structures SL1, SL2 with barrier thicknesses 2–3 nm, for structures SL3, SL4 with thicknesses in the range 2.5–3.5 nm.

4. Conclusion

An algorithm for calculating the energy of interband transitions for quaternary solid solutions based on „diluted“ nitrides is proposed in paper. Its main components were considered: calculation of the position of energy levels for given potentials of the edges of the conduction and valence bands, calculation of the band gap in the case of a quaternary solution based on „diluted“ nitrides, and an algorithm for estimating the hybridization parameter.

To test the developed algorithm, structures based on InGaAsN QWs were analyzed and the applicability of the algorithm was demonstrated by comparing the calculated values with the position of the PL spectrum peak, as well as with the results obtained using an alternative method for estimating the hybridization parameter. Based on the performed calculations, the parameters of layers of In(Ga)As/GaAsN superlattices were proposed for realizing active regions in the spectral range 1.3 μm.

Funding

The work of the authors from St. Petersburg National Research Academic University named after Zh.I. Alferov of the Russian Academy of Sciences was supported by a grant from the Russian Science Foundation No. 21-19-00718, https://rscf.ru/project/21-19-00718/ regarding the modeling of the band structure. The work of the authors from ITMO University was carried out with the financial support of the „Priority 2030“ program regarding the measurement of PL spectra.

Conflict of interest

The authors declare that they have no conflict of interest.

References

[1] C. Skierbiszewski, P. Perlin, P. Wisniewski, T. Suski, J.F. Geisz, K. Hingerl, W. Jantsch, D.E. Mars, W. Walukiewicz. Phys. Rev. B, **65** (3), 035207 (2001).
[2] A. Erol. *Dilute III–V Nitride Semiconductors and Material Systems* (Berlin–Heidelberg–N.Y., Springer Verlag, 2008).
[3] T. Sarmiento, Li Zhao, P. Moser, T. Li, Y. Huo, J.S. Harris. IEEE Phot. Techn. Lett., **31** (20), 1607 (2019).
[4] A.S. Gudovskikh, A.A. Lazarenko, E.V. Pirogov, M.S. Sobolev, K.S. Zelentsov, I.A. Morozov, A.Yu. Egorov. Semiconductors, **50** (5), 652 (2016).
[5] M. Henini. *Dilute nitride semiconductors* (Amsterdam–Boston–Heidelberg–London–N.Y.–Oxford–Paris–San Diego–San Francisco–Singapore–Sydney–Tokyo, Elsevier, 2005).
[6] Y. Onishi, N. Saga, K. Koyama, H. Doi, T. Ishizuka, T. Yamada, K. Fujii, H. Mori, J.Hashimoto, M. Shimazu, A. Yamaguchi, T. Katsuyama. IEEE J. Select. Topics Quant. Electron., **15** (3), 838 (2009).
[7] J. Vukusic, P. Modh, A. Larsson, M. Hammar, S. Mogg, U. Christiansson, V. Oscarsson, E. Odling, J. Malmquist, M. Ghisoni, P. Gong, E. Griffiths, A. Joel. Electron. Lett., **39** (8), 662 (2003).
[8] H. Riechert, A. Ramakrishnan, G. Steinle. Semicond. Sci. Techn., **17** (8), 892 (2002).
[9] G. Steinle, H. Riechert, A.Yu. Egorov. Electron. Lett., **37** (2), 93 (2001).
[10] M. Gębski, D. Dontsova, N. Haghighi, K. Nunna, R. Yanka, A. Johnson, R. Pelzel, J.A. Lott. OSA Continuum, **3** (7), 1952 (2020).
[11] A. Babichev, S. Blokhin, A. Gladyshev, L. Karachinsky, I. Novikov, A. Blokhin, M. Bobrov, N. Maleev, V. Andryushkin, E. Kolodeznyi, D. Denisov, N. Kryzhanovskaya, K. Voropaev, V. Ustinov, A. Egorov, H. Li, S. Tian, S. Han, G. Sapunov, D. Bimberg. IEEE Phot. Techn. Lett., **35** (6), 297 (2023).
[12] A.V. Babichev, L.Y. Karachinsky, I.I. Novikov, A.G. Gladyshev, S.A. Blokhin, S. Mikhailov, V. Iakovlev, A. Sirbu, G. Stepniak, L. Chorchos, J.P. Turkiewicz. IEEE J. Quant. Electron., **53** (6), 1 (2017).
[13] S. Blokhin, A. Babichev, A. Gladyshev, L. Karachinsky, I. Novikov, A. Blokhin, S. Rochas, D. Denisov, K. Voropaev, A. Ionov, N. Ledentsov, A. Egorov. Electron. Lett., **57**, 697 (2021).

[14] S.A. Blokhin, A.V. Babichev, A.G. Gladyshev, L.Ya. Karachinsky, I.I. Novikov, A.A. Blokhin, M.A. Bobrov, N.A. Maleev, V.V. Andryushkin, D.V. Denisov, K.O. Voropaev, I.O. Zhumaeva, V.M. Ustinov, A.Yu. Egorov, N.N. Ledentsov. IEEE J. Quant. Electron., **58** (2), 2400115 (2022).
[15] S.A. Blokhin, A.V. Babichev, A.G. Gladyshev, I.I. Novikov, A.A. Blokhin, M.A. Bobrov, N.A. Maleev, V.V. Andryushkin, D.V. Denisov, K.O. Voropaev, V.M. Ustinov. Opt. Eng., **61** (9), 096109 (2022).
[16] N.V. Kryzhanovskaya, A.I. Likhachev, S.A. Blokhin, A.A. Blokhin, E.V. Pirogov, M.S. Sobolev, A.V. Babichev, A.G. Gladyshev, L.Ya. Karachinsky, I.I. Novikov, V.V. Andryushkin, D.V. Denisov, A.Yu. Egorov. Laser Phys. Lett., **19** (7), 075801 (2022).
[17] M. Albrecht, V. Grillo, T. Remmele, H.P. Strunk, A.Yu. Egorov, Gh. Dumitras, H. Riechert, A. Kaschner, R. Heitz, A. Hoffmann. Appl. Phys. Lett., **81** (15), 2719 (2002).
[18] A.S. Dashkov, L.I. Goray. J. Phys.: Conf. Ser., **1410**, 012085 (2019).
[19] A.S. Dashkov, L.I. Goray. J. Semicond., **54**, 1823 (2020).
[20] C. Jirauschek, T. Kubis. Appl. Phys. Rev., **1** (1), 011307 (2014).
[21] I. Vurgaftman, J.R. Meyer, L.R. Ram-Mohan. J. Appl. Phys., **89** (11), 5815 (2001).
[22] A.R. Denton, N.W. Ashcroft. Phys. Rev. A, **43** (6), 3161 (1991).
[23] A.Yu. Egorov. Avtoref. dokt. dis. (SPb, SPbAU RAN, 2011).
[24] W. Shan, W. Walukiewicz, J.W. Ager III, E.E. Haller, J.F. Geisz, D.J. Friedman, J.M. Olson, Sarah R. Kurtz. J. Appl. Phys., **86** (4), 2349 (1999).
[25] Y.T. Lin, T.C. Ma, T.Y. Chen, H.H. Lin. Appl. Phys. Lett., **93** (17), 171914 (2008).
[26] A. Aho, M. Korpijärvi, R. Isoahoa, P. Malinen, A. Tukiainen, M. Honkanen, M. Guina. J. Cryst. Growth, **438**, 49 (2016).
[27] R. Isoaho, A. Aho, A. Tukiainen, T. Salminen, M. Guina. J. Cryst. Growth, **584**, 126574 (2022).
[28] R.J. Potter, N. Balkan. J. Phys. Condens. Matter, **16** (31), S3387 (2004).
[29] D. Alexandropoulos, M.J. Adams. IEE Proc. Optoelectron., **150** (2), 105 (2003).
[30] I. Vurgaftman, J.R. Meyer. J. Appl. Phys., **94** (6), 3675 (2003).
[31] S.A. Choulis, S. Tomic, E.P. O'Reilly, T.J.C. Hosea. Solid State Commun., **125** (3–4), 155 (2003).
[32] S.A. Choulis, T.J.C. Hosea, S. Tomic, M. Kamal-Saadi, A.R. Adams, E.P. O'Reilly, B.A. Weinstein, P.J. Klar. Phys. Rev. B, **66** (16), 165321 (2002).
[33] Z. Pan, L.H. Li, Y.W. Lin, B.Q. Sun, D.S. Jiang, W.K. Ge. Appl. Phys. Lett., **78** (15), 2217 (2001).
[34] A.Yu. Egorov, V.A. Odnoblyudov, N.V. Krizhanovskaya, V.V. Mamutin, V.M. Ustinov. Semiconductors, **36** (12), 1355 (2002).
[35] A. Polimeni, M. Capizzi, M. Geddo, M. Fischer, M. Reinhardt, A. Forchel. Phys. Rev. B, **63** (19), 195320 (2001).
[36] S.A. Choulis, T.J.C. Hosea, S. Tomic, M. Kamal-Saadi, B.A. Weinstein, E.P. O'Reilly, A.R. Adams, P.J. Klar. Phys. Status Solidi B, **235** (2), 384 (2003).
[37] H.D. Sun, M.D. Dawson, M. Othman, J.C.L. Yong, J.M. Rorison, P. Gilet, L. Grenouillet, A. Million. Appl. Phys. Lett., **82** (3), 376 (2003).
[38] W. Shan, W. Walukiewiez, J.W. Ager, E.E. Haller, J.F. Geisz, D.J. Friedman, J.M. Olson, S.R. Kurtz. Phys. Rev. Lett., **82** (6), 1221 (1999).
[39] P.J. Klar, H. Gruning, W. Heimbrodt, J. Koch, W. Stolz, P.M.A. Vicente, A.M. Kamal Saadi, A. Lindsay, E.P. O'Reilly. Phys. Status Solidi, **223** (1), 163 (2001).
[40] A. Lindsay, E.P. O'Reilly. Solid State Commun., **112** (8), 443 (1999).
[41] W. Shan, W. Walukiewicz, K.M. Yu, J.W. III Ager, E.E. Haller, J.F. Geisz, D.J. Friedman, J.M. Olson, S.R. Kurtz, H.P. Xin, C.W. Tu. Phys. Status Solidi, **223** (1), 75 (2001).
[42] I. Suemune, K. Uesugi, W. Walukiewicz. Appl. Phys. Lett., **77** (19), 3021 (2000).
[43] P. Perlin, P. Wisniewski, C. Skierbiszewski, T. Suski, E. Kaminska, S.G. Subramanya, E.R. Weber, D.E. Mars, W. Walukiewicz. Appl. Phys. Lett., **76** (10), 1279 (2000).
[44] C. Skierbiszewski, P. Perlin, P. Wisniewski, T. Suski, W. Walukiewicz, W. Shan, J.W. III Ager, E.E. Haller, J.F. Geisz, D.J. Friedman, J.M. Olson, S.R. Kurtz. Phys. Status Solidi, **216** (1), 135 (1999).
[45] P.J. Klar, H. Gruning, J. Koch, S. Schafer, K. Volz, W. Stolz, W. Heimbrodt, A.M. Kamal Saadi, A. Lindsay, E.P. O'Reilly. Phys. Rev. B, **64** (12), 121203 (2001).
[46] X. Yang, M.J. Jurkovic, J.B. Heroux, W.I. Wang. Appl. Phys. Lett., **75** (2), 178 (1999).
[47] E.D. Jones, N.A. Modine, A.A. Allerman, I.J. Fritz, S.R. Kurtz, A.F. Wright, S.T. Tozer, X. Wei. In *Light-Emitting Diodes: Research, Manufacturing, and Applications III* (San Jose, California, USA, 1999) v. 3621, p. 52.
[48] M. Kondow, T. Kitatani, S. Nakatsuka, M.C. Larson, K. Nakahara, Y. Yazawa, M. Okai, K. Uomi. IEEE J. Select. Topics Quant. Electron., **3** (3), 719 (1997).
[49] S. Tomic, E. O'Reilly, R. Fehse, S. Sweeney, A. Adams, A. Andreev, S. Choulis, T. Hosea, H. Riechert. IEEE J. Select. Topics Quant. Electron., **9** (5), 1228 (2003).
[50] A. Egorov, D. Bernklau, B. Borchert, S. Illek, D. Livshits, A. Rucki, M. Schuster, A. Kaschner, A. Hoffmann, Gh. Dumitras, M. Amann, H. Riechert. J. Cryst. Growth, **227–228** (1–4), 545 (2001).
[51] H. Riechert, A.Yu. Egorov, D. Livshits, B. Borchert, S. Illek. Nanotechnology, **11** (4), 201 (2000).
[52] R. Johnson, V. Blasingame, J. Tatum, B.S. Chen, D. Mathes, J. Orenstein, T.Y. Wang, J. Kim, Ho-Ki Kwon, J.H. Ryou, G. Park, E. Kalweit, H. Chanhvongsak, M. Ringle, T. Marta, J. Gieske. Proc. SPIE, **4994**, 222 (2003).
[53] G.L. Bir, G.E. Pikus. *Symmetry and Strain-Induced Effects in Semiconductors* (N.Y., Wiley, 1974).
[54] J.D. Cooper, A. Valavanis, Z. Ikonić, P. Harrison, J.E. Cunningham. J. Appl. Phys., **108** (11), 113109 (2010).
[55] C. Jirauschek. IEEE J. Quant. Electron., **45** (9), 1059 (2009).
[56] A.V. Babichev, E.V. Pirogov, M.S. Sobolev, D.V. Denisov, N.A. Fominykh, A.I. Baranov, A.S. Gudovskikh, I.A. Melnichenko, P.A. Yunin, V.N. Nevedemsky, M.V. Tokarev, B.Ya. Ber, A.G. Gladyshev, L.Ya. Karachinsky, I.I. Novikov, A.Yu. Egorov. FTP, **56** (10), 1002 (2022). (in Russian).
[57] A.V. Babichev, E.V. Pirogov, M.S. Sobolev, D.V. Denisov, H.A. Fominykh, A.I. Baranov, A.S. Gudovskikh, I.A. Melnichenko, P.A. Yunin, V.N. Nevedomsky, M.V. Tokarev, B.Ya. Ber, A.G. Gladyshev, L.Ya. Karachinsky, I.I. Novikov, A.Yu. Egorov. Semiconductors, **56** (10), 782 (2022).

[58] M.M. AI-Jassim, M.M. Goral, J.P. Sheldon, P. Jones, K.M. MRS Online Proc. Libr. (OPL), **144**, 183 (1988).
[59] A.M. Mintairov, T.H. Kosel, J.L. Merz, P.A. Blagnov, A.S. Vlasov, V.M. Ustinov, R.E. Cook. Phys. Rev. Lett., **87** (27), 277401 (2001).
[60] A. Babichev, S. Blokhin, E. Kolodeznyi, L. Karachinsky, I. Novikov, A.Egorov, S.C. Tian, D. Bimberg. Photonics, **10** (3), 268 (2023).
[61] J. Jewell, L. Graham, M. Crom, K. Maranowski, J. Smith, T. Fanning, M. Schnoes. Phys. Status Solidi C, **5** (9), 295 (2008).

Translated by E.Potapova